Pernas-Sánchez, J., Artero-Guerrero, J. A., López-Puente, J., & Varas, D. (2018). Numerical methodology to analyze the ice impact threat: Application to composite structures. Materials & Design, 141, 350-360.

doi:https://doi.org/10.1016/j.matdes.2017.12.044

Numerical methodology to analyze the ice impact threat: application to composite structures.

J. Pernas-Sanchez, J.A. Artero-Guerrero, J. López-Puente, D. Varas*

Department of Continuum Mechanics and Structural Analysis. University Carlos III of Madrid. Avda. de la Universidad, 30. 28911 Leganés, Madrid, Spain

Abstract

Impacts on composites produce interlaminar failure (delamination) which is difficult to detect in common maintenance tasks, and affects the structural integrity. Therefore it is critical, for safety, to improve prediction tools in order to perform tolerant damage designs. The numerical modelling of impacts of deformable objects (such as ice) on composite panels is still a challenge. Not only the modelling of the laminate should be appropriate to reproduce its behaviour and failures, but the modelling of the deformable projectile should be capable to induce the corresponding response and damages. In this work a two-step numerical methodology is proposed for the study of ice impact. First, the deformable impactor is analysed, studying the impact process on a rigid target (a steel plate attached to a load cell). Once the deformable projectile behaviour is fully captured, the ice impact on a deformable target (a carbon/epoxy laminate) is studied. The composite material model takes into account intralaminar and interlaminar failure in order to reproduce the laminate behaviour. Different ice sphere diameters ($30, 40$ and $50mm$) and impact velocities ($50 - 250\ m/s$) are considered in this study. All the results from the numerical simulations have been compared with the experimental results.

Keywords: Composite laminate; failure mechanism; delamination; Numerical

*corresponding author
Email address: dvaras@ing.uc3m.es; Fax/Phone:+34916248460 (D. Varas)

modeling; Ice behavior; impact.

1. Introduction

Fiber reinforced composites are, at present, one of the most common materials in aerospace and aeronautic industries. Its excellent stiffness/weight and strength/weight ratios make this type of materials one of the best choices to safe weight in structural parts; for example the main commercial aircraft constructor uses them in more than 50 % (in terms of weight) in his recent designs. Moreover these materials are able to safe manufacturing and maintenance times due to the ability to reproduce large pieces without joints. There are some drawbacks to these excellent properties: the brittle-like behavior of the composites increases the risk of sudden failure, and in addition they may present some damages (which affect the structural integrity) that are difficult to detect in common maintenance task. One of these damages could be the delamination produced by impacts, therefore the authorities have reported that kind of menace as a key factor in the design of composite structures: literally from an EASA 2011 report "*A critical safety issue for the design of primary aircraft structures is vulnerability and damage tolerance due to foreign object impact from bird strike, hail, tyre rubber and metal fragments*" [1].

Different authors have studied such type of events, from an experimental and a numerical point of view, using different kind of impactors. Hard projectile impacts (such as metal fragments) on composites have been studied experimentally since early 80's [2, 3, 4]; regarding the numerical approach, the development of reliable material models has allowed to analyse and to achieve a better understanding of these kind of events, examples of it can be found in [5, 6, 7, 8, 9, 10, 11, 12]. The literature about impact events using hard impactors are extensive due to the simplicity of testing and modeling a non-deformable projectile. The study and testing of deformable impactors is inherently more difficult, nevertheless it is possible to find studies regarding bird impacts [13, 14, 15], rubber impacts [16, 17, 18] or ice impacts [19, 20, 21], mainly from an experimental point of view.

Focusing on the experimental study of ice impacts, two different kind of works can be found in literature: those that study the ice impact against a rigid target and others that analyse the ice impact event onto a deformable target. The first group of works performs impacts of different ice geometries to obtain the impact force time history by means of a load cell or a Hopkinson tube. An example of these studies is the one carried out by Kim et al. [22], where a steel plate is attached to a load cell in order to measure the induced force produced by an ice sphere. The present authors published a previous work [23] in which impact tests on a load cell are performed to obtain the contact force, using a spring-mass model to reconstruct it, from the data measured by the load cell. Later Tippman et al. [24] used a Hopkinson tube to measure the impact force, by means of the unidimensional wave propagation theory, and hence avoiding the use of load cells. A different ice impactor geometry was studied by Pereira et al. [25] who performed tests to measure the impact force exerted by the impact of ice cylinders. The other mentioned group of works, which analyse the ice impact event onto a deformable target, can be subdivided attending the kind of target to be impacted: a metal (mainly aluminum) [21, 26] or a composite target [22, 27, 28, 29]. These kind of works analyse the deflection and damage appearance due to the ice impact, focusing in the interlaminar damage in the case of composites because it is the most important damage that appears. The present authors also studied in a previous experimental work [20] the influence of different ice sphere diameters impacting CFRP panels with different thickness.

Literature describing numerical models for the simulation of ice impact is likewise scarce. The first attempts to describe the constitutive behaviour of ice consisted on the use J2 elastoplastic models with different modes of failure [21, 30], which are mainly standard models available in commercial codes. Despite the simplicity of the mentioned models, the works showed its ability to capture some of the effects produced by ice impacts on different material plates. Nevertheless the models fail in the overall description of the ice behaviour during the impact. Later Carney et al. [31] developed a constitutive behaviour for the ice taking into account its strain rate sensitivity and the hydrostatic pressure dependence of ice, validating the model with experimental results of high velocity impacts of ice cylinders against a rigid plate [25]. Chuzel [32] used a constitutive equation based on the damage model of Mazars [33] and modified it to allow degradation in the strengths; the validation of the model was carried out with both impacts against a rigid plate and a deformable plate (aluminium panel). Recently, Tippmann et al. [24] proposed a J2 elastoplastic model with pressure cut-off and rate dependent yield strength, validating it with experimental test performed against a rigid plate.

Taking into account the different behaviour of a 'soft' or deformable projectile when impact onto a rigid or a deformable target, the differences of the impact process as well as the consequences in both cases, it is reasonable to think that any model proposed to describe the ice impact behaviour should require a wide validation to be on the security side. In this work a two-step numerical methodology is proposed for the study of the ice impact. First, the deformable impactor is analysed studying the impact process on a rigid target, thus the CFRP behaviour is not taken into account. A Drucker-Prager constitutive model with strain rate dependence for the ice is validated for impacts against a "rigid" target (a steel plate attached to a load cell). Once the deformable projectile behaviour is fully captured and the model validated, the study of ice impacts on a deformable target (a carbon/epoxy laminate) can be performed. The composite material model implemented takes into account both intralaminar and interlaminar failures in order to reproduce the laminate behaviour. Different ice sphere diameters and impact velocities are considered to study the force time histories induced on the load cell and the damage in composite laminates of different thickness.

In this work the authors propose a methodology with the aim of having a numerical model capable of reproducing the impact of a deformable projectile, on different kind of structures, and hence study its effects which could contribute in future design developments. The methodology consists firstly on analyze the ice impact behaviour on a "rigid" plate to validate the numerical model of the ice (a deformable projectile) and then study the ice impacts on a carbon/epoxy laminate (a deformable structure). It has been considered spherical ice projectiles to assure that the ice model is valid when different stress states appear on the projectile (compression and indirect tension) as well as a wide range of velocities in order to demonstrate its validity on different circumstances. In addition it is proposed a simplified CFRP model, in order to achieve a low computational cost, that predicts the damages that appear on the laminate and allows to analyze how they are produced during the impact process.

The first section of the article presents the material models for the composite laminate and the ice. Then, the experimental tests used for the validation are briefly explained (impacts on "rigid" plate and on composite laminate) as well as the numerical modeling developed. Finally, the validation of both types of impact and the results obtained in the numerical simulations are showed. The last section summarizes the main conclusions of the research.

2. Material modeling

The numerical methodology proposed in this work pursues to study the ice sphere impacts at different velocities onto different targets: steel plate and carbon/epoxy laminate. In this section the material models implemented for composite and ice are explained. The numerical methodology has been implemented using the commercial explicit finite element software LS-Dyna v.971 [34].

2.1. Ice material model

The ice material definition used in the numerical simulations consists on an hypoelastic, until failure, with strain rate dependence model. In order to capture the pressure dependence of the ice, a yield function based on a Drucker-Prager criterion [35], including strain rate dependence in the yield definition is considered. The model has been implemented in the commercial finite element code LS-Dyna v.971 [34] using an user subroutine.

The elastic behaviour is provided by the following expression of Hooke's law:

$$\dot{\sigma} = C : \dot{\varepsilon}^e = C : (\dot{\varepsilon} - \dot{\varepsilon}^p) \tag{1}$$

where $\dot{\sigma}$ is the objective rate of the Cauchy stress tensor, $\dot{\varepsilon}$ is the strain rate tensor, $\dot{\varepsilon}^e$ and $\dot{\varepsilon}^p$ the corresponding elastic and plastic the strain rate tensors, and C is the Hooke stress-strain tensor defined by the elastic constants.

The elastic regime defined is limited by a yield function, to this end the model assumes a Drucker-Prager yield function which includes the pressure dependence of the ice [36, 37] and the increasing trend of the compressive strength with strain rate. The Druker-Prager yield function (f_{DP}), defined in terms of equivalent stress ($\bar{\sigma}$) and the pressure (p) can be expressed as:

$$f_{DP} = \bar{\sigma} - (\sigma_{0y} + 3\alpha p) \tag{2}$$

where σ_{0y} is the material cohesion and α is a parameter related to the internal friction angle of the material. Both parameters may be related to the uniaxial stress limits in compression (σ_C) and in tension (σ_T):

$$\sigma_{0y} = \frac{2\sigma_C\sigma_T}{\sigma_C + \sigma_T} \qquad \alpha = \frac{\sigma_C - \sigma_T}{\sigma_C + \sigma_T} \tag{3}$$

so that the Drucker-Prager yield surface is completely defined once σ_T and σ_C are known. According to the experimental findings of several authors [19, 36, 38], the tensile strength is constant but the compressive strength is dependent on strain rate; hence the authors suggest a power law with strain rate sensitivity [39]:

$$\sigma_C\left(\dot{\bar{\varepsilon}}^p\right) = \sigma_{C0}\left(\frac{\dot{\bar{\varepsilon}}^p}{\dot{\bar{\varepsilon}}_0^p}\right)^m \tag{4}$$

being $\dot{\bar{\varepsilon}}^p$ the equivalent plastic strain rate, σ_{C0} the initial compressive strength and m, $\dot{\bar{\varepsilon}}_0^p$ material model's constant parameters.

To describe the inelastic flow, a non-associated plastic flow is proposed and integrated following the Kuhn-Tucker complementary condition and the consistency condition. Finally, two different pressure cut-offs were proposed for tension (P_T^{lim}) and compression (P_C^{lim}):

$$\begin{cases} p \ > P_T^{lim} = -\frac{\sigma_T}{3} \\ p \ < P_C^{lim} = \frac{\sigma_C}{3} \end{cases} \tag{5}$$

Once any of the pressure cut-off is reached, the deviatoric part of the stress is set to zero and the material only can withstand compressive hydrostatic stress. The parameters needed for the ice are obtained from the literature (Table 1).

Property	**Symbol**	**Magnitude**
Density	ρ	897.6 kg/m^3
Young's modulus	E	9.31 GPa
Poisson rate	ν	0.33
Initial compressive strength	σ_{C0}	10.976 MPa
Compressive strain rate sensitivity	m	0.0093783
Tensile strength	σ_{T0}	1.72 MPa

Table 1: Model parameters for ice. [39]

It is worth to mention that the ice model, briefly explained in this section, was proposed by the authors in a previous work to study ice cylinder impacts

[39], where further details about the model can be found. On that work, the model was validated using experimental results obtained from the work of Carney et al. [31]. In order to perform a wider validation of the ice numerical model, it has been considered necessary to validate it with a different ice geometry (an sphere), a wider range of impact velocities and impacting against a deformable target.

2.2. Carbon/epoxy laminate material model

In order to model the behaviour of the unidirectional carbon/epoxy laminate, different approaches are used to take into account both interlaminar and intralaminar failures. An orthotropic elastic material until failure is used to reproduce the intralaminar failure, whereas the interlaminar damage or delamination is modeled by means of the use of cohesive interactions. Both, material and cohesive interaction are available in the commercial code. A similar approach for high velocity impacts, obtaining good results, was adopted by the authors of the current work in previous articles [7, 40].

The intralaminar damage model considers different type of damages based in the Chang-Chang model [41]. Distinguishing between fiber and matrix failure for tension and compression, different variables e_i (based on stresses) are defined for each failure mechanism. When the value of any of these variables reaches the value of 0 ($e_i^2 \geq 0$), the material is unable to withstand more stress in this direction, instant in which the stiffness of the material involved in this failure mechanism is set to zero [42]. This sudden decrease of stiffness could promote excessive distortion, and thus numerical instabilities, which are mitigated removing the elements using a maximum strain criteria ($\varepsilon < 0.05$). The failure mechanisms are defined as a function of the stress tensor component (σ_{ij}) and the material strengths (X_i, Y_i, S_{12}).

Property	Symbol	Magnitude
Density	ρ	1580 kg/m^3
Young modulus 0°	E_1	139 GPa
Young modulus 90°	E_2	9.4 GPa
In-plane shear modulus	G_{12}	4.5 GPa
Poisson coefficient 12	ν_{12}	0.3089
Compressive strength 0°	X_c	1656 MPa
Tensile strength 0°	X_t	2105 MPa
Compressive strength 90°	Y_c	175 MPa
Tensile strength 90°	Y_t	79 MPa
Shear strength	S_c	114 MPa

Table 2: Carbon epoxy AS4/8552 properties from the manufacturer Hexcel

- Fiber failure:

$$e_f^2 = \begin{cases} \left(\frac{\sigma_{11}}{X_t}\right)^2 - 1 \ \ if \ \sigma_{11} > 0 \\ \left(\frac{\sigma_{11}}{X_c}\right)^2 - 1 \ \ if \ \sigma_{11} \leq 0 \end{cases} \tag{6}$$

- Matrix failure:

$$e_m^2 = \begin{cases} \left(\frac{\sigma_{22}}{Y_t}\right)^2 + \left(\frac{\sigma_{12}}{S_{12}}\right)^2 - 1 \ \ if \ \sigma_{11} > 0 \\ \left(\frac{\sigma_{22}}{2S_{12}}\right)^2 + \frac{\sigma_{22}}{Y_c}\left[\left(\frac{Y_c}{2S_{12}}\right)^2 - 1\right] + \left(\frac{\sigma_{12}}{S_{12}}\right)^2 - 1 \ \ if \ \sigma_{11} \leq 0 \end{cases} \tag{7}$$

The values of stiffness and strength are taken from the manufacturer Hexcel Composites and are listed in Table 2.

The interlaminar damage is taking into account through a cohesive interaction based on a traction-separation law, in which it is necessary to define a damage onset and a damage evolution law. Both define a relative displacement (δ) between the surfaces. This relative displacement is given as a function of the displacement between the surfaces in mode I ($\delta_I = \delta_3$) and in mode II ($\delta_{II} = \sqrt{\delta_1^2 + \delta_2^2}$), following the equation:

$$\delta_m = \sqrt{\delta_I^2 + \delta_{II}^2} \tag{8}$$

Property	Symbol	Magnitude
Maximum onset stress in mode I	T	35 MPa
Maximum onset stress in mode II	S	45 MPa
Coefficient in mixed mode	μ	1.45
Energy release rate in mode I	G_I	250 J/m
Energy release rate in mode II	G_{II}	750 J/m

Table 3: Cohesive interaction parameters.

The initiation criteria is function of the displacement of the softening onset (δ^0):

$$\delta^0 = \delta_I^0 \delta_{II}^0 \sqrt{\frac{1+\beta^2}{\left(\delta_{II}^0\right)^2 + \left(\beta \delta_I^0\right)^2}} \tag{9}$$

where $\delta_I^0 = T/E_N$ y $\delta_{II}^0 = S/E_T$ are the onset of softening in mode I and II, T and S are the peak stresses onset of softening in each mode; and E_N and E_T the stiffness of the different modes. Finally, $\beta = \delta_{II}/\delta_I$ is the ratio between the modes.

The ultimate displacement (δ^F) is defined as function of G_{IC} and G_{IIC} (the energy release rate for mode I and II respectively), and the power law coefficient (μ), Eq. 10. The properties used for the cohesive interaction can be seen in Table 3.

$$\delta^F = \frac{2\left(1+\beta\right)^2}{\delta^0} \left[\left(\frac{E_N}{G_{IC}} \right)^\mu + \left(\frac{E_T \cdot \beta^2}{G_{IIC}} \right)^\mu \right]^{-\frac{1}{\mu}} \tag{10}$$

3. Experimental tests for validation and numerical models

This section briefly describes the experimental tests used to validate the numerical methodology proposed, as well as the numerical models developed. The numerical modeling implemented pursues to reproduce the impacts of ice spheres onto a "rigid" and a deformable target. In order to validate and study the capacity of damage prediction of the model, different ice sphere diameters (30, 40 and 50 mm) and a wide range of impact velocities (from 50 to 250 m/s) were considered.

3.1. Ice sphere impact on steel plate with a load cell

3.1.1. Experimental tests

In order to observe how ice behaves under impact conditions, ice spheres of three different diameters (30, 40 and 50 mm) were launched against a load cell, measuring the force induced during the impact. The ice spheres were accelerated using a one stage light gas gun, which uses pressurized air to impel the projectile through a 5 meters long, 60 mm calibre barrel (Fig. 1). The impact velocity was varied from 50 to 250 m/s modifying the canon air pressure. A laser sensor placed between the barrel muzzle and the target allows to measure the ice velocity before the impact. In order to launch ice spheres of different diameter using a canon of 60 mm calibre, a foam sabot was designed to adjust the mismatch diameter, isolating and protecting the ice from the friction during the acceleration, avoiding melting. The aerodynamic design of the sabot allowed its separation from the ice projectile during the flight (using drag forces) before the impact. The ice sphere impacts on a cylindrical 200 mm diameter steel plate (Fig. 2) which is screwed to the load cell (model PB-2 manufactured by Microtest, designed to measure load under impact conditions) in order to measure the induced impact force. Finally, the steel plate-load cell group was held to a back structure as it is shown in Fig. 2. The data acquisition system employed to register the data measured by the load cell was a DEWETRON DEWE-800 system specifically designed for dynamic applications, capable to capture data up to 1MHz. In addition a Photron Ultima APX digital high-speed camera was used to record the impact, and to verify that the ice reached the load cell without losing its integrity; different frame rate was selected to record the impacts ranging from 18000 to 100000 fps. The lighting, in order to assure clear high-speed images, was provided by an Arrisun 12 Plus lamp head with a 1200 W Hydrargyrum Medium-arc Iodide (HMI) lamp.

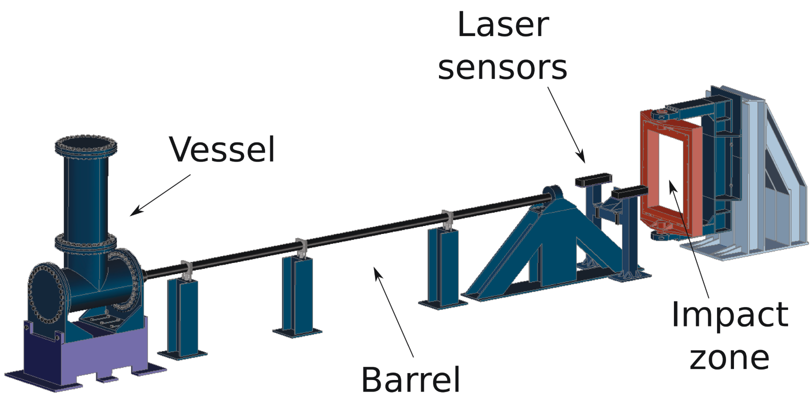

Figure 1: One stage light gas gun.

3.1.2. Numerical model

The numerical model reproduces the perpendicular impact of ice spheres against a steel plate attached to a load cell. The ice spheres are meshed with reduced integration hexahedral solid elements. After a mesh convergence study the number of element used for the 30, 40 and 50 mm ice diameter are 23625, 56000 and 109375 respectively, using a similar element size in all the cases. In a previous work [39], the authors explored the possibility of using an arbitrary lagrangian-eulerian mesh and a smooth particle hydrodynamic approximation to model the ice, but the results obtained by these techniques were similar to the results obtained by the lagrangian one, moreover this last technique was chosen because of its reduced computational cost. In order to avoid numerical instabilities due to large distortion suffered by the elements, a deletion criteria is implemented. This criteria is based on the equivalent strain; the maximum value has been chosen in order to not interfere with the simulations results

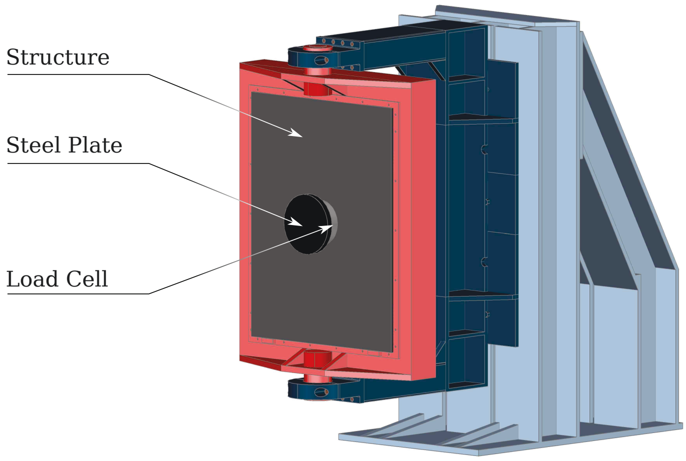

Figure 2: Steel plate, load cell and impact structure used in experimental tests.

($\bar{\varepsilon} = 1.5$).

Taking into account the experimental structure (steel plate-load cell-back structure) in which the ice spheres impact (Fig. 2), a spring-mass system with a steel plate has been used in the numerical simulations to reproduce the experimental set-up (Fig. 3). The steel plate is modeled, using hexahedral solid elements (3772 elements), as an elastic material ($\rho = 7850\,kg/m$, $E = 210\,GPa$ and $\nu = 0.3$) because no plastic deformation was observed. The other components of the load cell are modeled using unidimensional elements (springs) and masses with the values detailed in Table 4. These values have been obtained from the manufacturer specification and by modal analysis of the experimental facility [23].

Regarding the boundary conditions of the model, the end of spring k_1 is fixed and all the displacements, out of impact direction, in m_1, m_2 and the steel plate are impeded. In order to reproduce the impact velocity, an initial velocity was applied to the ice spheres. Finally, a penalty stiffness contact between the nodes of the spheres and the surface of the steel plate was defined.

Parameter	**Value**
m_1	$16.2\ Kg$
m_2	$17\ Kg$
Steel plate	$5.545\ Kg$
k_1	$1.61 \cdot 10^8\ N/m$
k_2	$1 \cdot 10^8\ N/m$
k_3	$3.7 \cdot 10^8\ N/m$

Table 4: Masses and springs to model the load cell system.

3.2. Ice sphere impact on CFRP panel

3.2.1. Experimental tests

A campaign of ice impact tests on CFRP panels was carried out in order to study how this kind of impacts may affect these composite structures, widely used in the aeronautic industry. Two different ice diameters (40 and 50 mm) were launched against laminates at velocities ranging from 50 to 250 m/s. In order to perform the tests, the launcher previously described was used (Fig. 1).

In this case, the ice impacts on square plates of 300 mm side with two different thickness: 4 and 6 mm approximately (21 and 32 plies respectively) with the ply sequence presented in Table 5. The laminates were clamped to the rig structure located in the impact zone (Fig. 1) using a screwed steel frame, leaving a free span of 280×280 mm. The impact event was recorded by means of a high speed camera (Photron Ultima APX); the lighting, as in the case of the ice impacts on a steel plate, was provided by an HMI lamp. A set-up scheme of the experiments can be observed in Fig. 4. In addition, some of the composite plates were monitored during the impact using strain gauges. The strain gauges were located on the back face at $30\,mm$ away from the impact point; each gauge measures the strain in the direction parallel to the side of the plate, as it is showed in Fig. 4. Once the impact was performed, the composite laminate

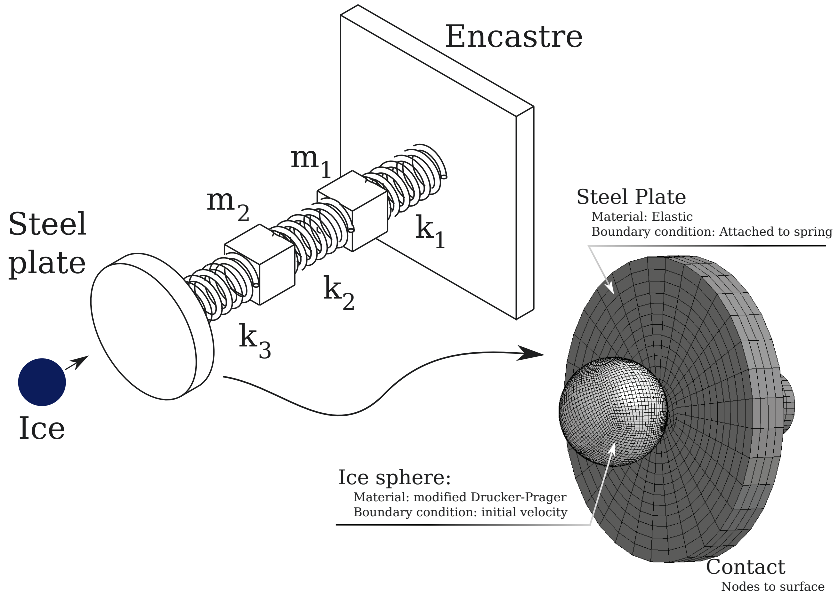

Figure 3: Steel plate and load cell system used in the numerical simulations

was inspected using ultrasonic techniques in order to measure the interlaminar damage extension.

Laminate	**Ply sequence**	**Thickness**
21 Plies	$(45/-45/90/0/90/-45/45/90/0/90/0)S'$	3.9 mm
32 Plies	$(45/-45/90/0/90/-45/45/90/0/90/45/-45/90/90/-45/45)S$	6.0 mm

Table 5: Ply sequence of laminates used.

3.2.2. Numerical model

In this case, the numerical model reproduces the experimental tests in which ice spheres impact perpendicularly against a composite panel. The model pursues to study the capability of the numerical method to predict the effects of an ice impact on a CFRP structure. The ice sphere model is identical to the one previously detailed.

The two different thickness (4 and 6 *mm*) square composite plates afore-

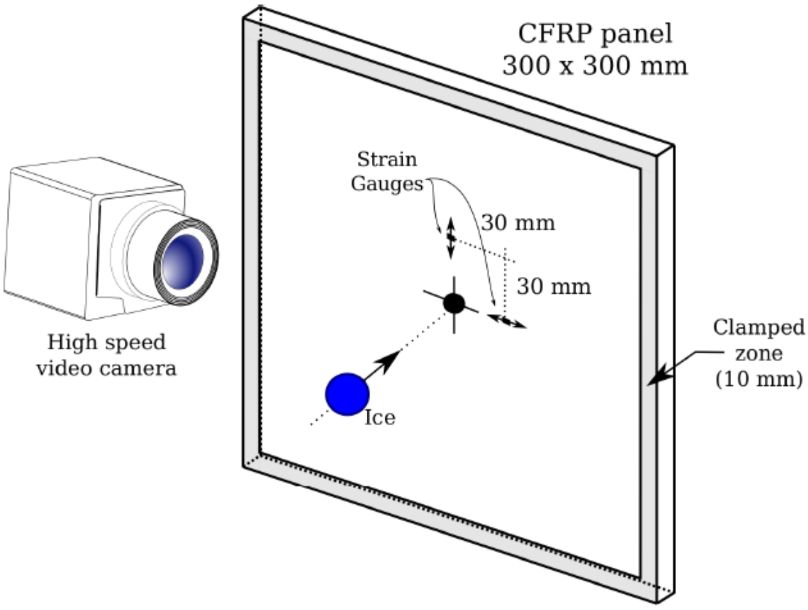

Figure 4: Experimental scheme.

mentioned are modeled, as it has been already explained, taking into account intralaminar failures by means of the material model considered and the interlaminar failures by means of cohesive interactions (Fig. 5). In order to reduce the high computational cost that induces to have a cohesive interaction between each ply of the laminate, clusters of plies were used, including a cohesive interaction between these groups of plies. This approach was used by the authors of the current article on previous works where composite laminates were subjected to high velocity impacts, obtaining good results [7, 40]. The configuration of clusters, including the cohesive interaction ($/\leftrightsquigarrow/$) between the plies with mismatch angle orientation and in clusters of 7 plies for the 21 plies laminate and clusters of 8 plies in the case of 32 plies laminate, is the following:

- 21 plies: $(\underbrace{45/-45/90/0/90/-45/45}/\leftrightsquigarrow/\underbrace{90/0/90/0})S'$
- 32 plies: $(\underbrace{45/-45/90/0/90/-45/45/90}/\leftrightsquigarrow/\underbrace{0/90/45/-45/90/90/-45/45})S \rightsquigarrow$

The discretization has been done using hexahedral shell elements (thick shell elements in LS-Dyna notation), each cluster was meshed with 4900 thick shell elements (and a Gauss point for each ply), resulting in 14700 (102900 Gauss points) and 19600 (156800 Gauss points) elements for the 21 and 32 plies laminates respectively, determined after a mesh convergence study. Regarding the boundary conditions of the model, the laminate sides were clamped (The 6 DOF were restricted along the 280x280 mm plates sides). Finally, as in the case of impacts on a steel plate a penalty stiffness contact between the nodes of the spheres and the laminate surface was defined.

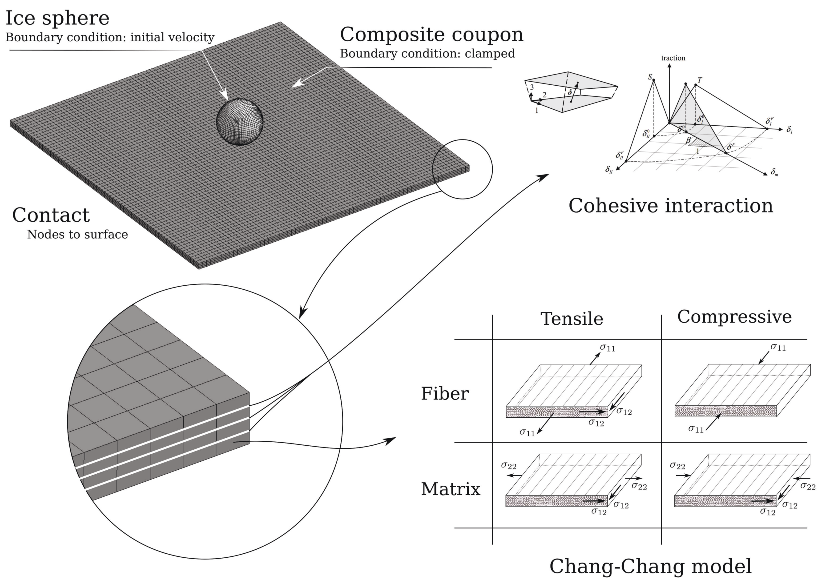

Figure 5: Finite element model built for the numerical simulation of ice impact against composite laminates.

4. Validation and discussion

This section shows the validation of the numerical methodology developed in order to study the ability of the numerical simulation to reproduce the behaviour and effects of an ice impact, as well as its capacity of damage prediction on composite panels. The results of experimental ice impacts on a steel plate (with a load cell) are mainly used to validate the ice model proposed. Once validated the ice modeling, it can be used to study the ice impact effects on a composite laminate, in particular the appearance of damage. The experimental and numerical results are compared and analysed.

4.1. Ice sphere impacts on steel plate with load cell

The model of ice used in this work was previously validated [39], as it was already mentioned, using experimental results of ice cylinders impacting against a load cell [31]. The stress state promoted by the impact in a cylinder is completely different to the one that appears in an sphere. In a slender cylinder the stress state is close to uniaxial compression whereas in a sphere, both compression and indirect tension appears. Therefore in order to assure that the proposed model can reproduce the ice behaviour on different circumstances, it has been considered appropriate to extend the validation to a different ice geometry (spheres) and in a wide range of impact velocities.

The force time history, obtained experimental and numerically (Force in k_3 in Fig. 3), of impacts with two different ice diameter and impact velocities are shown in figures 6(a) and 6(b). The ice diameter and impact velocities were selected in order to show extreme values of kinetic energies (low velocity-small diameter & high velocity-large diameter) and hence observe the differences or similarities on the whole range of energies considered. The experimental and numerical curves show a good agreement between them: a sudden increase of the force at the beginning of impact followed by a gentle small plateau, and finally a slope to reach the maximum force value. Not only the trend, but also the maximum value is well predicted. In addition, the pulse force duration produced by the ice impact is predicted correctly by the numerical simulations and hence the final impulse is well reproduced.

The maximum force values, experimental and numerically obtained, for all

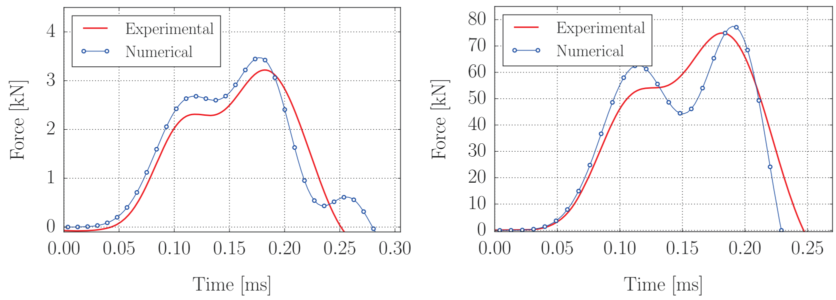

(a) 30 mm ice sphere at 67 m/s (b) 50 mm ice sphere at 211 m/s

Figure 6: Experimental and numerical force time histories for impacts of different ice spheres at different velocities.

the ice diameters and impact velocities are shown in Fig. 7. It can be observed that the maximum force varies from less than 5 kN to more than 85 kN, for the cases with a higher kinetic energy. Fig. 7 also shows how the maximum force increases as the impact velocity raises and how the slope of the force curve raises when the diameter is bigger. As it can be seen, the numerical model not only predicts adequately the maximum force values, but capture the aforementioned trends. According to this fact, it could be said that the model is capable of reproducing the physical phenomena that appears in the impact process of an ice for complex stress fields.

In order to study the ice impact phenomenon, not only the force induced by the ice projectile should be predicted by the numerical simulations, but also the general behaviour of the material should be represented. Ice impactors flow over the structure, spreading the impact load; thus for a reliable damage prediction of impact it is necessary that the numerical model predicts faithfully how the ice deforms during the impact. Fig. 8 shows different frames of the high-speed video recorded during the impact (18000 fps), at a velocity of 115 m/s, of an ice sphere with a diameter of 40 mm and the corresponding numerical frames. It can be observed that the numerical model is capable of reproducing, qualitatively, the spreading of the ice along the steel plate as the impact develops.

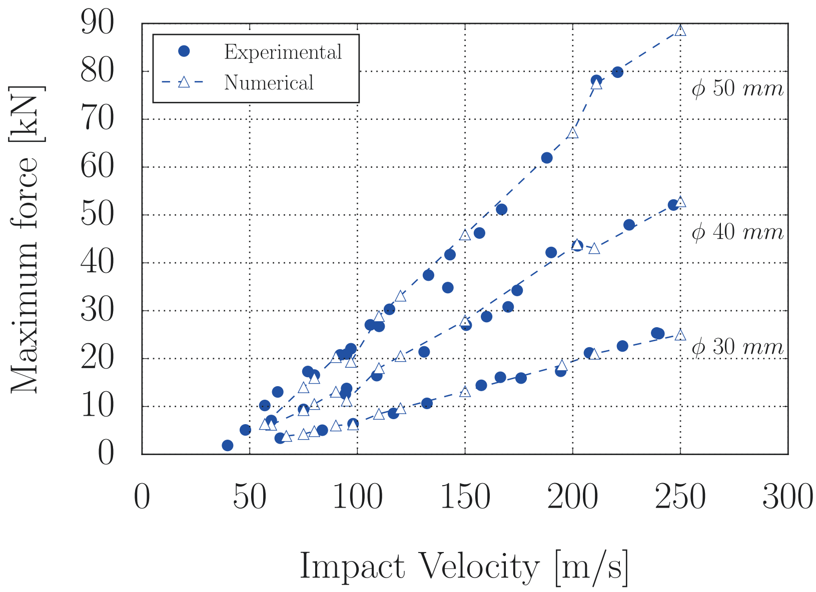

Figure 7: Experimental and numerical maximum forces against impact velocity

The images of the impact recorded by the high speed camera show how the ice becomes white at the beginning of the impact ($t = 55\ \mu s$). This is due to the appearance of cracks inside the projectile [23]. In order to estimate the failure or fragmentation process given by the numerical simulations, an internal variable of failure (which indicates when the behaviour of the ice is out of the elastic regime) is defined to evaluate if the numerical model represents faithfully the ice behaviour. Fig. 9 compares the numerical and experimental images of the impact process (recorded at 100000 fps), focusing on the failure process evolution. The upper part of the images represents the contour plot of the defined failure internal variable, whereas the bottom part of the images shows how the experimental fragmentation evolves, according to the whiteness of the fragmented zone [23]. Although the numerical simulation does not fragment as the ice does, it can be said that the numerical model is able to reproduce the failure development during the impact.

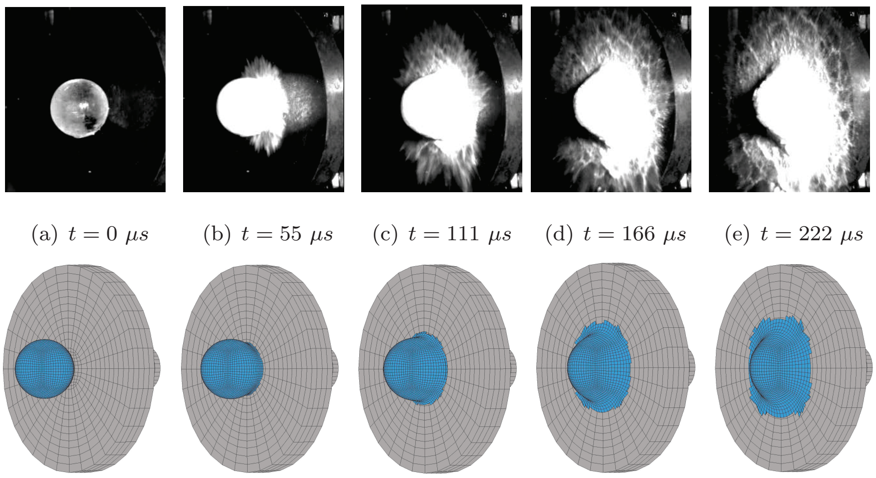

(a) $t = 0\ \mu s$ (b) $t = 55\ \mu s$ (c) $t = 111\ \mu s$ (d) $t = 166\ \mu s$ (e) $t = 222\ \mu s$

(f) $t = 0\ \mu s$ (g) $t = 55\ \mu s$ (h) $t = 111\ \mu s$ (i) $t = 166\ \mu s$ (j) $t = 222\ \mu s$

Figure 8: Comparison between numerical and experimental images of a 40 mm ice diameter projectile impacting at 115 m/s.

According to the observed result it is possible to state that the strain suffered by the ice during the impact is small before the aforementioned failure variable is activated, therefore it can be concluded that defining properly the elastic regime of the ice model becomes capital to obtain good numerical results. The overall predicted behaviour of the ice is in accordance with the statement of other authors that propose an embrittlement with the strain rate of the ice [37, 43, 44]. Taking into account the results obtained it is possible to state that the proposed ice model, based on a Drucker-Prager criterion with strain rate dependence, predicts faithfully this region of the failure process.

According to the aforementioned results, it can be concluded that the ice material model is validated, not only for ice cylinders [39] but, also for ice sphere impacts. In addition, the numerical results show the capability of the lagrangian approach to reproduce the impact phenomena. The validation performed enable the use of the model proposed to analyse more complex problems.

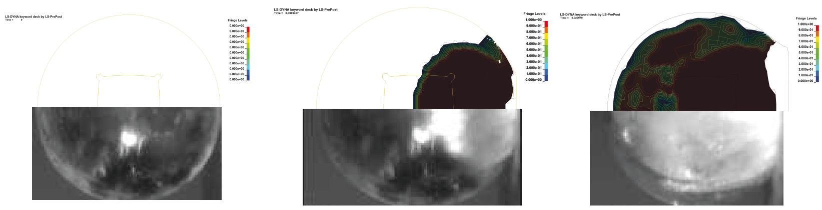

$t = 0\,\mu s$ $t = 9.52\,\mu s$ $t = 19.04\,\mu s$

Figure 9: Failure development during the impact experimental and numerical comparison.

4.2. Ice sphere impacts on CFRP panel

Once the ice model is validated, it can be used to validate and study ice impacts on composite panels. The goal of this second group of numerical simulations is to demonstrate that the numerical model developed is able to capture the appearance of the damage in composite laminates subjected to ice impact and that it can be a useful tool to analyse and design structures under this kind of events.

Prior to study numerically the damages induced in the laminates by the ice impact, the overall behaviour of the plates is studied by means of the strain gauges measurements. Fig. 10 shows the strain experimentally measured and predicted by the numerical simulations, for a 21 plies laminate impacted by a 40 mm ice sphere at 157 m/s. At the beginning of the impact, the ice promotes a compression wave followed by a plate bending; this behaviour can be measured by the strain gauges. The numerical simulations reproduce the overall trends and the values measured. It is observed that the magnitude of the compression wave is underestimated, probably because of the use of a continuum shell approach. However, the tension magnitude and decay as well as the intervals of change between compression and tension are well captured by the numerical model proposed.

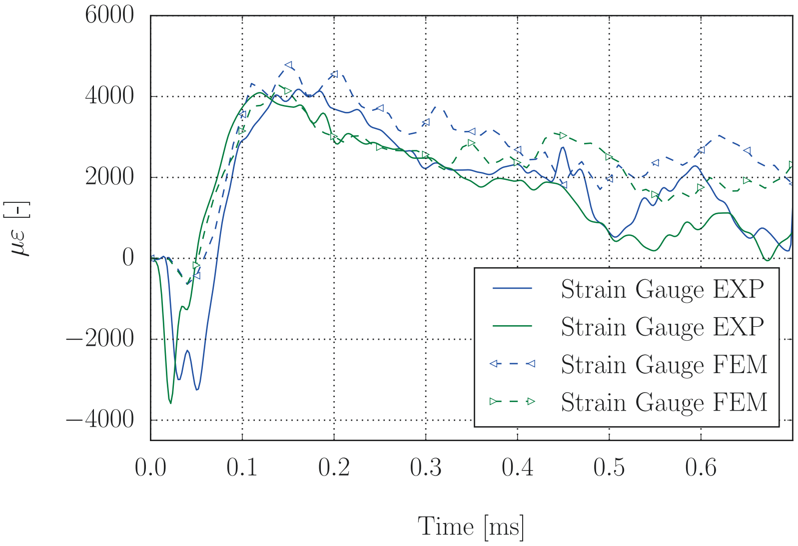

Figure 10: Experimental and numerical measurements of the strain gauges for an impact of 40 mm diameter ice sphere against 21 plies laminate at 157 m/s

In order to verify if the composite material model is reproducing accordingly the behaviour of the impacted laminate panel, the different kind of failures that may appear are studied, comparing the numerical and experimental results. The model implemented is able to capture intralaminar damages, such as fiber breakage or matrix cracking, and interlaminar failures (delaminations) through the presence of cohesive interactions. The intralaminar damages barely can be observed, making difficult the comparison between numerical and experimental results: in the simulations hardly progress from the impact point, and experimentally only can be visualized in the cases impacted at high kinetic energy. Nevertheless, the interlaminar damage is spread out over the laminate from the impact point and can be perfectly quantified. Figs. 11 and 12 show the experimental (C-Scan) and numerical results of delamination in two laminates impacted at different velocities; the areas colored in red denote interlaminar damages. Qualitatively comparing the results, it can be observed that in both cases the numerical model predicts adequately the extension and shape of the delamination. At low impact velocity (Fig. 11) the delamination spreads around the impact zone, which is well reproduced by the numerical model although it has to be said that, in this case, the numerical results underestimate slightly the delaminated area. When the panel is impacted at higher velocity (215 m/s) (Fig. 12) the interlaminar damage spreads out from the impact point over almost the whole free area, only the zones near the clamped boundaries do not show delamination; this phenomenon is well reproduced by the numerical model.

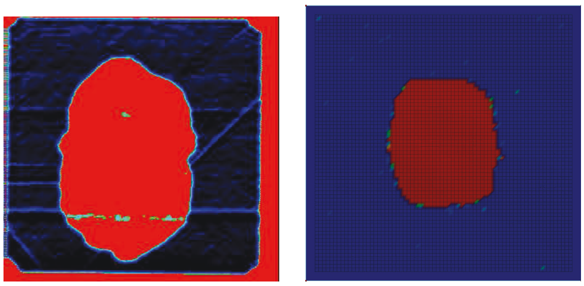

(a) Experimental (b) Numerical

Figure 11: Experimental and numerical delamination for an impact of 40 mm ice diameter impacting against a 21 plies laminate at 157 m/s. (For interpretation of the references to colour in this figure legend, the reader is referred to the web version of this article.)

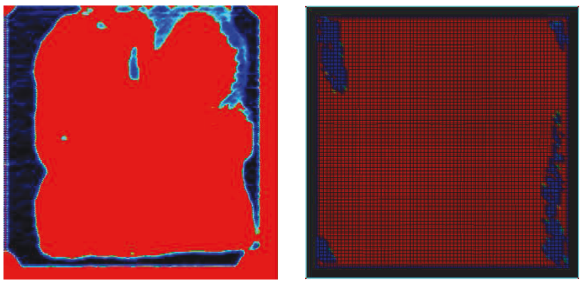

(a) Experimental (b) Numerical

Figure 12: Experimental and numerical delamination for an impact of 40 mm ice diameter impacting against a 21 plies laminate at 215 m/s. (For interpretation of the references to colour in this figure legend, the reader is referred to the web version of this article.)

In order to compare quantitatively the interlaminar failure, Fig. 13 depicts the percentage of delaminated area versus the impact velocity for all the ice sphere diameters (40 and 50 mm) and laminate thicknesses (4 and 6 mm) tested. In all cases it is observed a sudden transition between zero delamination to full delamination, which can be considered when the delaminated area is greater than 75% (red lines in Fig. 13). This transition occurs at a different impact velocity, which will be called critical velocity from now on, for each ice sphere diameter-laminate thickness combination. It can be seen how the numerical model is able to capture this behaviour for each combination, although the experimental results show a sharper transition than the numerical results. The influence of the ice sphere diameter and panel thickness, in the critical velocity, is also well reproduced by the numerical model. It is observed that, for the same panel thickness, it is necessary a higher impact velocity to reach full delamination with a smaller ice diameter. For a given ice diameter, the impact velocity that produces the full delamination is higher on the thicker panel.

Taking into account the validation and the study carried out for different kind of ice impacts, it can be said that the numerical method proposed is capable of reproducing faithfully the behaviour of the ice subjected to an impact, and the effects that it can produce onto a "rigid" and flexible target for different ice diameters and panel thickness. In addition, it has been demonstrated that the numerical model can predict the delaminations caused by an ice impact on a composite panel, being a useful tool to analyse this kind of events.

Once validated, the numerical methodology proposed could be used as a design tool previous to the manufacturing phase, or even to analyse some aspects of these impact events that experimentally could be very difficult, or unable to perform. Fig. 14 shows numerical results of the delamination and displacement evolution in a thin laminate (4 mm) impacted by an ice sphere of 40 mm at 175 m/s. The displacement of the laminate centre increases suddenly at the beginning of the impact, as delamination does. Then, the displacement reaches a small plateau, while delamination continues growing, followed by the maxi-

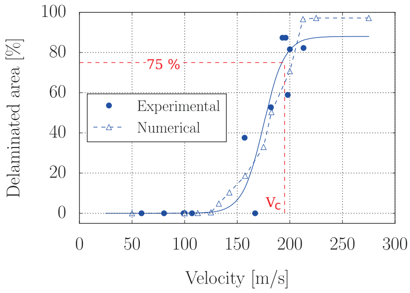

(a) $t = 4\ mm\ \phi =\ 40\ mm$

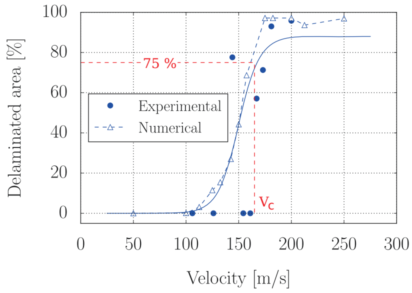

(b) $t = 4\ mm\ \phi =\ 50\ mm$

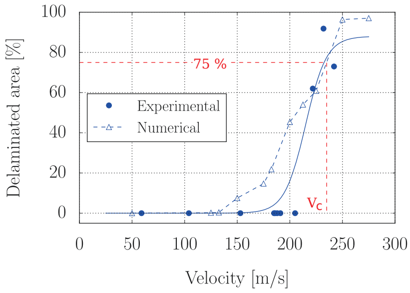

(c) $t = 6\ mm\ \phi =\ 40\ mm$

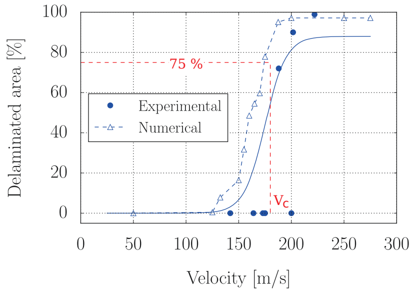

(d) $t = 6\ mm\ \phi =\ 50\ mm$

Figure 13: Experimental and numerical percentage of delaminated area against impact velocity for the two plate thickness and different projectile diameter.

mum displacement. It is reasonable to think that the peak force induced by the ice impact is reached at that instant. From that point, the displacement diminishes while delamination continues spreading out slowly. Therefore it can be said that the timing of delamination and displacement are directly related and that the main part of the delaminated area is produced at the beginning of the impact.

5. Conclusions

In this work a numerical methodology has been proposed to predict the behavior and threat of ice sphere projectiles impacting at high velocity. To this end a two step validation approach has been performed. Firstly, simulations of

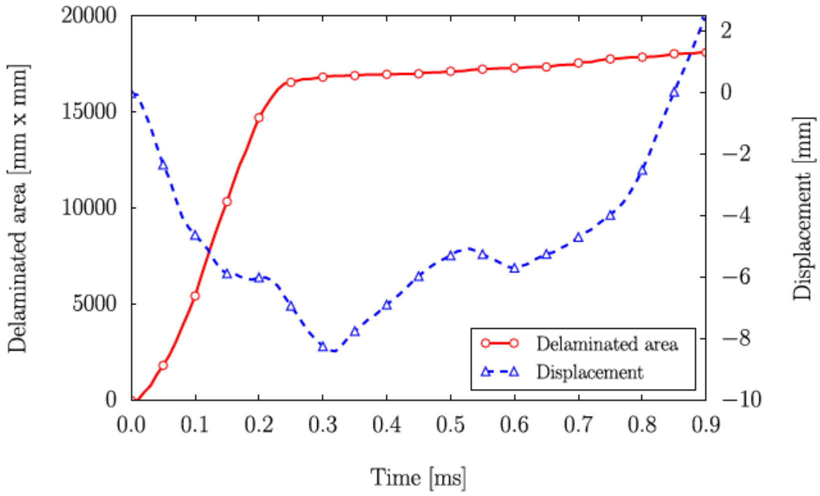

Figure 14: Center panel displacement and delamination evolution for an impact of 40 mm ice diameter impacting against a 21 plies laminate at 175 m/s.

high velocity impacts have been carried out in a wide range of impact velocities, for different ice diameters against a steel plate with a cell load, measuring and comparing the impact force produced by the ice spheres. Moreover, the progression of failure inside the ice was also validated. Once the material model has been proved reliable, the ice model has been used to simulate an impact event on carbon/epoxy laminates. To this end, different ice diameters have been impacted against carbon/epoxy laminates, studying the damages induced and comparing it with the experimental results. The main conclusions are as follows:

- The ice model implemented reproduces faithfully the behaviour of the ice subjected to an impact, and the effects that it can produce, for multiple conditions and test set-ups ("rigid" and flexible target). The input to the model is based on clearly defined mechanical properties.
- Regarding the numerical modeling of the laminate panel; the strategy of clustering the plies, reducing the interfaces in which delamination may appear, proves to be feasible to reproduce the delaminated area.

- The numerical model is able to reproduce the behaviour of composite panels impacted by an ice sphere, for all the combinations ice spheres-laminate thickness studied. The numerical model provides, faithfully, the critical velocity in which the laminate suffers an intense interlaminar failure.

- The validated numerical model has allowed to study the displacement and delamination evolution. The results show a direct relation between them and that the main part of the delaminated area is produced at the beginning of the impact.

- It has been proved that the numerical methodology proposed can be a useful tool to study or design composite structures that may be subjected to this kind of impacts.

Acknowledgements

This research was done with the financial support of the Spanish Ministry of Economy and Competitiveness under Project reference DPI2013-41094-R, and the Vicerrectorado de Política Científica UC3M (Projects 2014/00006/002 and 2013/00413/002).

References

[1] J. A. Toso N, LIBCOS-Load upon impact behaviour of composite Structure Research Project EASA.2009/3, Tech. rep., European Aviation Safety Agency (2011).

[2] W. Cantwell, J. Morton, Detection of impact damage in CFRP laminates, Compos. Struct. 8223 (3) (1985) 241–257.

[3] W. Cantwell, J. Morton, Geometrical effects in the low velocity impact response of CFRP, Compos. Struct. 8223 (89).

[4] W. Cantwell, J. Morton, Comparison of the low and high velocity impact response of cfrp, Composites 20 (1989) 545–51.

[5] J. López-Puente, R. Zaera, C. Navarro, Experimental and numerical analysis of normal and oblique ballistic impacts on thin carbon/epoxy woven laminates, Composites Part A 39 (2) (2008) 374–387.

[6] A. F. Johnson, A. K. Pickett, P. Rozycki, Computational methods for predicting impact damage in composite structures., Compos. Sci. Technol. 61 (2001) 2183–92.

[7] J. Pernas-Sánchez, J. Artero-Guerrero, J.Zahr Viñuela, D. Varas, J. López-Puente, Numerical analysis of high velocity impacts on unidirectional laminates, Compos. Struct. 107 (2014) 629 – 634.

[8] V. Lopresto, V. Melito, C. Leone, G. Caprino, Effect of stitches on the impact behaviour of graphite/epoxy composites, Compos. Sci. Technol. 66 (2) (2006) 206 – 214.

[9] J. López-Puente, R. Zaera, C. Navarro, The effect of low temperatures on the intermediate and high velocity impact response of CFRPs., Composites Part B 33 (2002) 559–66.

[10] W. B., J. Xiong, X. Wang, L. Ma, G. Zhang, L. Wu, J. Feng, Energy absorption efficiency of carbon fiber reinforced polymer laminates under high velocity impact, Materials & Design 50 (Supplement C) (2013) 140 – 148. doi:https://doi.org/10.1016/j.matdes.2013.01.046.

[11] Q. Ang, F. Kunkun, L. Wei, Z. Chengbi, T. Youhong, Modelling low-speed drop-weight impact on composite laminates, Materials & Design 60 (Supplement C) (2014) 520 – 531. doi:https://doi.org/10.1016/j.matdes.2014.04.041.

[12] Shaktivesh, N. Nair, C. Sesha Kumar, N. Naik, Ballistic impact performance of composite targets, Materials & Design 51 (Supplement C) (2013) 833 – 846. doi:https://doi.org/10.1016/j.matdes.2013.04.093.

[13] J. Wilbeck, Impact behavior of low strength projectiles, Tech. Rep. AFML-TR-77-134, Air Force Materials Laboratory (1978).

[14] L. Nizampatnam, Models and methods for bird strike load predictions, Ph.D. thesis, Wichita State University (2007).

[15] T. Baughn, L. Graham, Simulation of a birdstrike impact on aircraft canopy material, Journal of Aircraft 25 (1988) 659–664.

[16] D. Karagiozova, R. Mines, Impact of aircraft rubber tyre fragments on aluminium alloy plates: II - Numerical simulation using LS-DYNA, Int. J. Impact Eng. 34 (2007) 647–667.

[17] R. Mines, S. McKown, R. Birch, Impact of aircraft rubber tyre fragments on aluminium alloy plates: I-experimental, Int. J. Impact Eng. 34 (2007) 627–646.

[18] P. Guégan, R. Othman, D. LeBreton, F. Pasco, N. Swiergiel, P. Thevenet, Experimental investigation of rubber ball impacts on aluminium plates, Int. J. Crashworthiness 15 (2010) 391–399.

[19] H. Kim, J. N. Keune, Compressive strength of ice at impact strain rates, Journal of Materials Science (full set) September 2007 (2007) 2802–2806.

[20] J. Pernas-Sánchez, J. A. Artero-Guerrero, D. Varas, López-Puente, Experimental analysis of ice sphere impacts on unidirectional carbon/epoxy laminates, Int. J. Impact Eng. 96 (2016) 1 – 10.

[21] M. Anghileri, F. Invernizzi, M. Mascheroni, A survey of numerical models for hail impact analysis using explicit finite element codes, Int. J. Impact Eng. 31 (2005) 929–944.

[22] H. Kim, D. A. Welch, K. T. Kedward, Experimental investigation of high velocity ice impacts on woven carbon/epoxy composite panels, Composites Part A 34 (2003) 25–41.

[23] J. Pernas-Sánchez, J. A. Artero-Guerrero, D. Varas, J. López-Puente, Analysis of ice impact process at high velocity, Exp. Mech. 55 (9) (2015) 1669–1679.

[24] J. Tippmann, H. Kim, J. Rhymer, Experimentally validated strain rate dependent material model for spherical ice impact simulation, Int. J. Impact Eng. 57 (2013) 43–54.

[25] J. M. Pereira, S. A. Padula, D. M. Revilock, M. E. Melis, Forces Generated by High Velocity Impact of Ice on a Rigid Structure, Tech. Rep. July, NASA (2006).

[26] A. Combescure, Y. Chuzel-Marmot, J. Fabis, Experimental study of high-velocity impact and fracture of ice, Int. J. Solids Struct. 48 (20) (2011) 2779–2790.

[27] G. J. Appleby-Thomas, P. J. Hazell, G. Dahini, On the response of two commercially-important CFRP structures to multiple ice impacts, Compos. Struct. 93 (10) (2011) 2619–2627.

[28] L. Asp, R. Juntikka, High velocity impact on NCF reinforced composites, Compos. Sci. Technol. 43 (2009) 1478–82.

[29] J. Rhymer, H. Kim, D. Roach, The damage resistance of quasi-isotropic carbon/epoxy composite tape laminates impacted by high velocity ice, Composites Part A 43 (7) (2012) 1134–1144.

[30] H. Kim, K. T. Kedward, Modeling Hail Ice Impacts and Predicting Impact Damage Initiation in Composite Structures, AIAA Journal 38 (7) (2000) 1278–1288.

[31] K. Carney, D. Benson, P. Dubois, R. Lee, A phenomenological high strain rate model with failure for ice, Int. J. Solids Struct. 43 (25-26) (2006) 7820–7839.

[32] Y. Chuzel, Caractérisation expérimentale et simulation numérique d impacts de glace a haute vitesse., phdthesis (2009).

[33] J. Mazars, G. Pijaudier Cabot, Continuum damage theory application to concrete, Journal of Engineering Mechanics 115 (2) (1989) 345–365.

[34] L. S. TECHNOLOGY, LS-Dyna KEYWORD USER ' S MANUAL v.971, Livermore, California, rev 5 Edition (2010).

[35] D. C. Drucker, W. Prager, Soil mechanics and plastic analysis or limit design, Q J Applied Mathematics X (2) (1952) 157–165.

[36] M. Shazly, V. Prakash, B. A. Lerch, High strain-rate behavior of ice under uniaxial compression, Int. J. Solids Struct. 46 (6) (2009) 1499–1515.

[37] E. Schulson, Brittle failure of ice, Eng. Fract. Mech. 68 (2001) 1839–87.

[38] S. J. Jones, High Strain-Rate Compression Tests on Ice, The Journal of Physical Chemistry B 101 (32) (1997) 6099–6101.

[39] J. Pernas-Sánchez, D. Pedroche, D. Varas, J. López-Puente, R. Zaera, Numerical modeling of ice behavior under high velocity impacts, Int. J. Solids Struct. 49 (14) (2012) 1919–1927.

[40] D. Varas, J. Artero-Guerrero, J. Pernas-Sánchez, J. López-Puente, Analysis of high velocity impacts of steel cylinders on thin carbon/epoxy woven laminates, Compos. Struct. 95 (2013) 623–629.

[41] F. K. Chang, K. Y. Chang, A Progressive Damage Model for Laminated Composites Containing Stress Concentrations, J. Compos. Mater. 21 (834).

[42] H. Hahn, S. Tsai, On the Behavior of Composite Laminates After Initial Failures, J. Compos. Mater. 8 (3) (1974) 288–305.

[43] R. Juntikka, R. Olsson, Experimental and modelling study of hail impact on composite plates, in: 17th INTERNATIONAL COMMITTEE ON COMPOSITE MATERIALS, 2009.

[44] E. Schulson, The brittle compressive fracture of ice, Acta Metall. Mater. 38 (10) (1990) 1963 – 1976.